CERN-TH/2000-265

Intercepts of the non-singlet structure functions

B.I. Ermolaev

A.F. Ioffe Physico-Technical Institute, 194021 St.Petersburg, Russia

M. Greco

CERN, 1211 Geneva 23, Switzerland

and

Dipartimento di Fisica and INFN, University of Rome III, Rome, Italy

S.I. Troyan

Petersburg Nuclear Physics Institute, 188300 Gatchina, St.Petersburg, Russia

Abstract

Infrared evolution equations for small-x behaviour of the non-singlet structure functions f_1^{NS} and g_1^{NS} are obtained and solved in the next-to-leading approximation, to all orders in α_s, and including running α_s effects. The intercepts of these structure functions, i.e. the exponents of the power-like small-x behaviour, are calculated. A detailed comparison with the leading logarithmic approximation (LLA) and DGLAP is made. We explain why the LLA predictions for the small-x dependence of the structure functions may be more reliable than the prediction for the Q^2 dependence in the range of Q^2 explored at HERA.

I. INTRODUCTION

In recent years the deep inelastic scattering (DIS) of leptons off hadrons has been the object of intensive theoretical studies. In QCD the hadronic tensor for electron proton DIS

is usually regarded as a convolution of two objects: the "partonic" tensor $W_{\mu\nu}$ describing DIS off a (nearly) on-shell parton (quark or gluon) and the probability P_h^p to find the parton in the nucleon. As is well known, they have a different description: whereas the tensor $W_{\mu\nu}$ can be calculated within perturbation theory, there are no model-independent methods of calculating P_h^p, but only the general behaviour with respect to the kinematical variables can be predicted. Usually, the hadronic tensor $W_{\mu\nu}$ is presented in terms of the structure functions (see e.g. [1]) $f_{1,2}$ and $g_{1,2}$:

$$W_{\mu\nu} = \left(-g_{\mu\nu} + \frac{q_\mu q_\nu}{q^2}\right) f_1 + \left(p_\mu - \frac{(pq)}{q^2} q_\mu\right)\left(p_\nu - \frac{(pq)}{q^2} q_\nu\right) \frac{1}{(pq)} f_2 + \imath \epsilon_{\mu\nu\lambda\sigma} \frac{m q^\lambda}{(pq)} \left[S^\sigma g_1 + \left(S^\sigma - \frac{(Sq)}{pq} p^\sigma\right) g_2\right], \quad (1)$$

where p, m, S are the momentum, mass and polarization of the incoming parton and q is the momentum of the virtual photon. The structure functions depend on the Bjorken variable $x = -q^2/(2pq)$, with $(1 > x > 0)$ and $Q^2 = -q^2 > 0$. Each of the structure functions consists of flavour singlet and flavour non-singlet (NS) contributions. Although the singlet contributions accounting for gluon splitting are dominant at small x, the NS contributions are also interesting quantities to investigate. They can be expressed in terms of densities of quarks (Δq) and antiquarks ($\Delta\bar{q}$) inside a hadron. The non-singlet spin-dependent structure function g_1^{NS} refers to the combination of $(\Delta q + \Delta\bar{q})$, whereas the non-singlet spin-averaged structure function f_1^{NS} is related to $(\Delta q - \Delta\bar{q})$; combining them one could study the evolution of Δq and $\Delta\bar{q}$ separately.

The standard theoretical investigation of DIS structure functions, originally developed for the kinematic region of $x \sim 1$ and large Q^2, is made through the DGLAP [2] evolution equations . This approach accounts for the evolution of the structure functions with respect to the photon virtuality Q^2, whereas the evolution with respect to x is neglected. In other words, the DGLAP accounts for the resummation of all powers of $\ln Q^2$ and systematically neglects the powers of $\ln x$, which is obviously correct when x is not small. Despite the fact that the DGLAP equations provide a good agreement with experimental data (see e.g. [3]), they are not expected to work well in the small-x region, where logarithms of x are not

less important than logarithms of Q^2 and therefore must be taken into account to all orders in α_s. This resummation leads to a power-like, or Regge-like, behaviour in x and in Q^2 of the type $f_1^{NS} \propto (\sqrt{Q^2}/x)^a$. Such a behaviour cannot be obtained within DGLAP, which predicts a dependence of the type $f_1^{NS} \propto \exp\sqrt{c\ln(1/x)\ln\ln Q^2}$.

In perturbative QCD the power-like behaviour was obtained long ago [4] for the singlet structure functions of spin-averaged DIS and later in refs. [5,6] for the structure functions g_1 and f_1^{NS}. However, contrary to the DGLAP, the results of refs. [4–6] are obtained in the leading logarithmic approximation (LLA) with a fixed QCD coupling α_s. Hence the exponents calculated in [4–6] (also called intercepts) for the predicted power-like small-x behaviour of all structure functions contain α_s fixed at a scale that is not well defined. The very existence of such a scale, sometimes called "a reasonable scale", and estimates for its numerical value have been discussed in many works (see e.g. [7]). However, according to the Regge theory, the expressions for the intercepts must not contain α_s running with Q^2, but, on the contrary, they just have to be numbers.

Thus, in order to obtain realistic values for the intercepts, one has to go beyond the LLA and include the QCD running coupling effects in the evolution equations at small x, so that the running coupling α_s would be integrated out in the solutions. Recently in ref. [8] we have obtained expressions for the non-singlet structure function[1] f_1^{NS}, with running QCD coupling effects taken into account. The resulting intercept does not explicitly depend on α_s but depends on the infrared cut-off. That calculation prompted us to study the running QCD coupling effects for the non-singlet structure functions in more detail.

The structure function g_1^{NS} is similar to f_1^{NS}, because the same Feynman graphs contribute to both of them. As a result, they obey the same leading order (LO) DGLAP evolution equation. A difference between them arises only in next-to-leading order (NLO) corrections to DGLAP and can be extracted from the expressions of the second loop anoma-

[1] f_1^{NS} was denoted as f^{NS} in work [8].

lous dimensions (see e.g. [9,10]).

Concerning the small-x behaviour, the difference between f_1^{NS} and g_1^{NS} can be related to the difference in their signatures: the signature of f_1^{NS} is positive whereas g_1^{NS} has a negative one. A difference between them means that some high-order non-ladder graphs contribute to f_1^{NS} and g_1^{NS} in a different way. Historically, signatures for scattering amplitudes of high energy processes were first introduced in the context of the Regge theory (see e.g. [11]). A forward scattering amplitude $M(s,u)$, where s and u are the Mandelstam variables, has positive (negative) signature if it is symmetrical (antisymmetrical) with respect to the replacement $s \leftrightarrow u$:

$$M^{(+)}(u,s) = M^{(+)}(s,u), \qquad M^{(-)}(u,s) = -M^{(-)}(s,u). \tag{2}$$

Basically, any forward scattering amplitude $M(s)$ consists of the two parts:

$$M(s,u) = M^{(+)} + M^{(-)}, \qquad M^{(\pm)} = \frac{1}{2}\left(M(s,u) \pm M(u,s)\right). \tag{3}$$

In the small-x region, neglecting $O(m^2/s)$ and $O(Q^2/s)$ terms, one can use $u \approx -s$. As the imaginary part in s, $\Im_s M$, for $s > 0$, corresponds to the cross-section, this cross-section may acquire contributions from both $M^{(+)}$ and $M^{(-)}$ amplitudes. The partonic tensor $W_{\mu\nu}$ of Eq. (1) can be considered as the imaginary part of the amplitude $M_{\mu\nu}$ of the forward Compton scattering of a virtual photon on a constituent quark:

$$\begin{aligned} M_{\mu\nu} = &\left(-g_{\mu\nu} + \frac{q_\mu q_\nu}{q^2}\right) 2M_1 + \left(p_\mu - \frac{(pq)}{q^2}q_\mu\right)\left(p_\nu - \frac{(pq)}{q^2}q_\nu\right)\frac{1}{(pq)}2M_2 \\ &+ \imath\epsilon_{\mu\nu\lambda\sigma}\frac{mq^\lambda}{(pq)}\left[S^\sigma 2M_3 + \left(S^\sigma - \frac{(Sq)}{pq}p^\sigma\right)2M_4\right], \end{aligned} \tag{4}$$

so that

$$W_{\mu\nu} = \frac{1}{2\pi}\Im_s M_{\mu\nu}, \tag{5}$$

and in particular,

$$f_1 = \frac{1}{\pi}\Im_s M_1, \qquad g_1 = \frac{1}{\pi}\Im_s M_3\ . \tag{6}$$

The amplitude $M_{\mu\nu}$ is invariant with respect to the replacement $q \to -q$, $\mu \leftrightarrow \nu$ which corresponds to the crossing transition from the s-channel to the u-channel. However, the projection operators multiplying f_1 and g_1 behave differently under such a transition: the operator $(g_{\mu\nu} - q_\mu q_\nu/q^2)$ does not change, so the invariant amplitude M_1 multiplying it does not either. On the contrary, the operator $(\imath\epsilon_{\mu\nu\lambda\sigma} m q_\lambda/(pq))$ acquires a negative sign, so the invariant amplitude M_3 must acquire a negative sign too. Therefore, the invariant amplitudes

$$M^{(+)} = \frac{1}{2}\left(M_1(s,u) + M_1(u,s)\right) \tag{7}$$

and

$$M^{(-)} \equiv \frac{1}{2}\left(M_3(s,u) - M_3(u,s)\right) \tag{8}$$

have positive and negative signatures, respectively, and the DIS structure functions f_1 and g_1 can be considered as imaginary parts of scattering amplitudes with positive and negative signatures:

$$f_1 = \frac{1}{\pi}\Im_s M^{(+)} \ , \qquad g_1 = \frac{1}{\pi}\Im_s M^{(-)} \ . \tag{9}$$

The first observation of the importance of the contribution of the negative-signature amplitudes to the cross-sections was made in the context of QED in ref. [12]. Later on, in ref. [13], quark-quark scattering amplitudes with positive and negative signatures were calculated in the double-logarithmic approximation (DLA). Using the results of those works, it was shown in ref. [6] that in DLA, with α_s fixed, the intercept of g_1^{NS} is larger than the intercept of f_1^{NS}.

In the present paper we obtain explicit expressions for f_1^{NS} and g_1^{NS} for small values of x, which account for both leading double-logarithmic (DL) and sub-leading single-logarithmic (SL) contributions to all orders in QCD coupling, including running α_s effects. As logarithms of both x and Q^2 are important at small x, we account for both of them, constructing and solving a two-dimensional infrared evolution equation (IREE). In order to take running α_s

effects into account, we use the approach of ref. [13], with the improvement made in our previous work [8]. Also, we discuss similarities and differences between running α_s effects in the DGLAP and in our approach. Finally we discuss the region of applicability of the LLA and estimate the range of Q^2 where it can be safely applied. The paper is organized as follows: in Section 2 we derive the small-x evolution equations for the non-singlet structure functions and solve them. In Section 3 we obtain the asymptotic behaviour of f_1^{NS} and g_1^{NS}. In Section 4 we compare our results with the intercepts of the non-singlet structure functions obtained in LLA. In Section 5 our findings are compared with DGLAP predictions for the NS anomalous dimensions and we discuss the difference in accounting for running α_s effects. Finally, Section 6 contains our conclusions.

II. SMALL-X EVOLUTION EQUATION FOR THE NON-SINGLET STRUCTURE FUNCTIONS

In the Born approximation, which is the pure NS case, $M_{\mu\nu}$ is given by the sum of the graphs in Fig. 1. They yield

$$M_{\mu\nu}^{Born} = \left(-g_{\mu\nu} + 2x\frac{p_\mu p_\nu}{(pq)}\right) 2M_{Born}^{(+)} + \left(\imath\epsilon_{\mu\nu\lambda\sigma}\frac{mq^\lambda}{(pq)}S^\sigma\right) 2M_{Born}^{(-)}, \tag{10}$$

where

$$M_{Born}^{(\pm)} = e_q^2\frac{1}{2}\left[\frac{s-m^2-q^2}{m^2-s-\imath\epsilon} \pm \frac{u-m^2-q^2}{m^2-u-\imath\epsilon}\right], \tag{11}$$

with e_q being the electric charge of the incoming quark and $s=(p+q)^2$, $u=(p-q)^2$ the Mandelstam variables. We have omitted unimportant contributions proportional to q_μ, q_ν in Eq. (10).

$M_{Born}^{(\pm)}$ are amplitudes of defined signature (cf. Eq. (2)). Obviously, only the first term in Eq. (11), corresponding to the graph (a) in Fig. 1, has an imaginary part in s at $s>0$, which gives the same contribution to the amplitudes of both signatures. According to Eq. (9) we obtain the well-known results:

$$f_1^{Born} = g_1^{Born} = \frac{e_q^2}{2}\delta(1-x) \ . \tag{12}$$

The property $f_1^{Born} = g_1^{Born}$ remains true in the next one-loop approximation, with one gluon added to graphs in Fig. 1. Only the dressing of graph (a) in Fig. 1 contributes to the imaginary part in s at $s > 0$. This explains why the LO DGLAP splitting functions and the LO anomalous dimensions are the same for the structure functions corresponding to amplitudes with different signatures. The difference between them arises only at the second-loop order. Indeed, let us consider graph (a) of Fig. 2. It is actually a non-ladder graph, obtained from the Born graph (b) in Fig. 1 by adding two gluons to it. On the other hand, graph (a) in Fig. 2 can be redepicted as graph (b) in Fig. 2. It is easy to check that its imaginary part in s (the quark propagators to be cut are marked with crosses in Fig. 2) has, in particular, DL terms ($\sim \ln^3(1/x)$); this graph therefore cannot be neglected. Then, one can see that the DL contribution of this graph, which is symmetrical in μ, ν (contribution to f_1^{NS}) and the antisymmetrical one (contribution to g_1^{NS}) have different signs. This example shows that some higher-loop contributions to f_1^{NS} and g_1^{NS} are different.

Thus, a possible regular way of calculating f_1^{NS} and g_1^{NS} consists of the following steps:

(i) Calculate the forward scattering Compton amplitude $M_{\mu\nu}$ obtained by adding gluon propagators to both Born graphs in Fig. 1.

(ii) Extract from it the amplitudes M_1 and M_3 proportional to $(-g_{\mu\nu})$ and $\imath\epsilon_{\mu\nu\lambda\sigma}q^\lambda p^\sigma/(pq)$ (cf. Eqs. (4) and (6)), which are the positive- and negative- signature amplitudes $M^{(\pm)}$, respectively.

(iii) Calculate $(1/\pi)\Im_s M^{(\pm)}$.

So, first we calculate $M_{\mu\nu}$, and we do it by constructing and solving an IREE for $M_{\mu\nu}$. In order to account for the evolution in both x and Q^2 one must consider DL and SL contributions to all orders in α_s. High order Feynman graphs contributing to $M_{\mu\nu}$ may have both ultraviolet (UV) and infrared (IR) singularities. Whereas UV singularities are

absorbed by renormalization, IR ones must be regulated explicitly. Providing gluons with a mass violates the gauge invariance. In order to save it and to avoid IR singularities, we use the Lipatov prescription of compactifying the impact parameter space (see e.g. works [14,13,15]). In other words, we introduce the infrared cut-off μ in the transverse space (with respect to the plane formed by q and p) for integrating over the momenta of virtual particles:

$$k_{i\perp} > \mu \ . \tag{13}$$

With such a cut-off acting as a mass scale, one can neglect quark masses and still be free from IR singularities. As a result the amplitude $M_{\mu\nu}$ depends on the cut-off and we can study its evolution with respect to it, thus obtaining the IREE for $M_{\mu\nu}$. Feynman graphs contributing to the non-singlet structure functions are obtained from graphs in Fig. 1 by adding gluon propagators to them, without breaking the quark lines, however. With logarithmic accuracy, the region of integration over transverse momenta of virtual quarks and gluons can be regarded for every Feynman graph contributing to $M_{\mu\nu}$ as a sum of sub-regions so that in every sub-region only one virtual particle (quark or gluon) has the minimal transverse momentum $k_\perp$. We call such particles the softest ones although their longitudinal momenta can be large (see e.g. [15]). It is essential that integrating over $k_\perp$ one includes μ as the lowest limit. The softest particle can be either a gluon or a quark. When the softest particle is a quark, DL contributions come from the sub-region where another quark has the same transverse momentum, so that there appears a t-channel intermediate state with a soft quark pair. Therefore in order to keep the DL contributions, one must consider $M_{\mu\nu}$ as convolution of two amplitudes connected by the softest quark pair, each quark with the minimal transverse momentum $k_\perp$, as depicted by graph (b) in Fig. 3. The first amplitude appearing in graph (b) (the upper blob) is the Compton forward scattering $M_{\mu\nu}$ and the second one (the lower blob) is the forward scattering amplitude of quarks M_0. On the other hand, when the particle with the minimal $k_\perp$ is a virtual gluon, it can be factorized out of the amplitude with the DL accuracy [16]. This means, in particular, that the propagator of such softest gluon is attached to external lines only, yielding zero result. Having added the Born

contribution to the convolution graph (b) in Fig, 3, we arrive at the equation of the Bethe - Salpeter type for $M_{\mu\nu}$. As usual the Bethe - Salpeter equation relates $M_{\mu\nu}$ with on-shell quarks (lhs of equation in Fig. 3) to $M_{\mu\nu}$ with off-shell quarks (rhs of Fig. 3). However, all amplitudes in Fig. 3 are actually on-shell because the virtual quark pair in Fig. 3 has the minimal transverse momentum $k_\perp$. Integrations in blobs imply $k_\perp$ to be a new IR cut-off and, therefore, a new mass scale for these blobs (see [13,15,16]).

Let us note that in the DGLAP approach such softest quark pair is always in the lowest ladder rung because of the DGLAP ordering: in this approach all ladder transverse momenta $k_{i\perp}$ are indeed ordered as

$$\mu \leq k_{1\perp} \leq k_{2\perp} \leq ... \leq Q^2, \tag{14}$$

the numeration running from the bottom of the ladder to the top. Equation (14) shows that only the integration over $k_{1\perp}$ has μ as the lower limit. The lower limits for other $k_{i\perp}$ with $i \neq 1$ are expressed through the other transverse momenta. Therefore the small-x DGLAP equations correspond to the case where the quark scattering amplitude in graph (b) in Fig. 3 is considered in the Born approximation. As is well known, the ordering of Eq. (14) corresponds to accounting for $\ln^n(Q^2/\mu^2)$ without considering terms $\ln^m(1/x)$ not accompanied by logarithms of Q^2. On the other hand, as we investigate the small-x region, we have to lift this ordering, allowing for the transverse momentum of quarks in any ladder rung to reach the lowest limit $k_\perp = \mu$. Obviously, this increases the region of integration over $k_{i\perp}$. Then, a quark pair with minimal $k_\perp$ appears in any rung of the ladder Feynman graph.

The convolution of the amplitudes depicted in graph (b) prompts us to apply the Mellin transform for solving this equation. However, to respect the signatures of $M^{(\pm)}$ it is more convenient to use the asymptotic form of the Sommerfeld - Watson (SW) transform (see [11]):

$$M^{(\pm)}(\frac{s}{\mu^2}, \frac{Q^2}{\mu^2}) = \int_{-\imath\infty}^{\imath\infty} \frac{d\omega}{2\pi\imath} \left(\frac{s}{\mu^2}\right)^\omega \xi^{(\pm)}(\omega) F^{(\pm)}(\omega, \frac{Q^2}{\mu^2}), \tag{15}$$

where

$$\xi^{(\pm)} = -\frac{e^{-\imath\pi\omega} \pm 1}{2} \tag{16}$$

is the signature factor, for which this transform differs from that of Mellin. The inverse transform to Eq. (15) is

$$F^{(\pm)}(\omega) = \frac{2}{\sin(\pi\omega)} \int_0^\infty d\rho \exp(-\omega\rho) \Im_s M^{(\pm)}(\rho), \tag{17}$$

where $\rho = \ln(s/\mu^2)$.

The small-x region corresponds effectively to the dominance of the small-ω region in Eq. (15). Expanding ξ into series in ω and retaining the first terms in Eq. (15, $\xi^{(+)} \approx -1 + \imath\pi\omega/2$ and $\xi^{(-)} \approx \imath\pi\omega/2$, we see that in the small-x (or small-ω) region

$$\frac{1}{\pi}\Im_s M^{(\pm)} = \frac{1}{2}\int_{-\imath\infty}^{\imath\infty} \frac{d\omega}{2\pi\imath} \left(\frac{s}{\mu^2}\right)^\omega \omega F^{(\pm)}(\omega, \frac{Q^2}{\mu^2}); \tag{18}$$

we need to calculate $F^{(\pm)}$ only to obtain the structure functions f_1^{NS} and g_1^{NS} (cf. Eq.(6)). To do this one can apply the SW transform of Eq. (15) to the equation depicted in Fig. 3 and then differentiate it with respect to $\ln \mu^2$. On the other hand the Born amplitude does not depend on μ and therefore vanishes when differentiated with respect to μ. Then, observing that

$$-\mu^2 \frac{\partial M^{(\pm)}}{\partial \mu^2} = \frac{\partial M^{(\pm)}}{\partial \ln(s/\mu^2)} + \frac{\partial M^{(\pm)}}{\partial \ln(Q^2/\mu^2)} \tag{19}$$

corresponds to

$$\omega F^{(\pm)} + \frac{\partial F^{(\pm)}}{\partial y} \tag{20}$$

for the amplitudes $F^{(\pm)}$, where we have defined $y = \ln(Q^2/\mu^2)$, and differentiating the rhs of the equation depicted in Fig. 3 with respect to $\ln \mu^2$, we are led to the following IREE :

$$\left(\frac{\partial}{\partial y} + \omega\right) F^{(\pm)}(\omega, y) = \left[\frac{1}{8\pi^2}(1 + \lambda\omega)\right] F^{(\pm)}(\omega, y) F_0^{(\pm)}(\omega) \quad , \tag{21}$$

where $\lambda = 1/2$. For more details, see ref. [8], where the latter equation was obtained for $F = F^{(+)}$. The only difference now is that IREE (21) involves also the negative signature

amplitude $F_0^{(-)}$ of forward quark - quark scattering instead of $F_0^{(+)}$ only. The solutions to Eq. (21) are

$$F^{(\pm)} = C \exp\left(\left[-\omega + (1+\lambda\omega)F_0^{(\pm)}(\omega)/8\pi^2\right] y\right) \quad , \tag{22}$$

which contain two unknown quantities. The first one is an arbitrary factor C, essentially of a non-perturbative nature, which can be fixed by comparison with the data.

The other unknown quantity $F_0^{(\pm)}$ can be specified by constructing and solving the IREE for the amplitude M_0 of forward scattering of quarks. The equation for M_0 is shown in Fig. 4. The first two terms in the rhs look similar to the equation in Fig. 3. Indeed, the rhs consists of the Born contribution depicted by graph (a), the convolution of two quark scattering amplitudes (graph (b)), the intermediate quarks having minimal transverse momenta $k_\perp$, and a new contribution depicted by graphs (c) - (f). For symmetry, the contributions of graphs (c) and (d) are equal. The same is true for graphs (e) and (f). All these graphs correspond to the case where the particle with the minimal transverse momentum $k_\perp$ is a gluon. The propagators of such soft gluons are attached to external lines because by integrating over the soft gluon momenta the most singular DL contributions come from the region where each soft virtual gluon is factorized out (see e.g. ref. [16]). Self-energy graphs are absent in Fig. 4 because the Feynman gauge is used. The blobs in these graphs imply integrations over momenta of internal virtual particles with $k_\perp$ acting as a new IR cut-off. Let us consider in detail the contribution of the graphs in the rhs of the equation in Fig. 4. The Born contribution coming from graph (a) in Fig. 4 is given by

$$B^{(\pm)} = -2\pi C_F \left[\alpha_s(s)\frac{s}{s-\mu^2+\imath\epsilon} \pm \alpha_s(-s)\frac{-s}{-s-\mu^2+\imath\epsilon}\right], \tag{23}$$

where the quark mass is substituted by μ in the denominator and is suppressed in the numerator as well as $-q^2$. We use for α_s the following formula:

$$\begin{aligned}\alpha_s(s) &= \frac{1}{b\ln(-s/\Lambda^2_{QCD})} = \frac{1}{b\left[\ln(s/\Lambda^2_{QCD}) - \imath\pi\right]} \\ &= \frac{1}{b}\left[\frac{\ln(s/\Lambda^2_{QCD})}{\ln^2(s/\Lambda^2_{QCD})+\pi^2} + \frac{\imath\pi}{\ln^2(s/\Lambda^2_{QCD})+\pi^2}\right],\end{aligned} \tag{24}$$

where $b = (33 - 2n_f)/12\pi$ (n_f – the number of flavours).

Equation (24) is written in such a way that $\alpha_s(s)$ has non-zero imaginary part when s is positive. Applying the transform Eq. (17) to Eq. (23) we define

$$R^{(\pm)} = \frac{2}{\pi\omega}\int_0^\infty d\rho \exp(-\omega\rho)\Im_s B^{(\pm)}(\rho) = \frac{A}{\omega}, \tag{25}$$

where $\rho = \ln(s/\mu^2)$,

$$A(\omega) = \frac{4C_F\pi}{b}\left[\frac{\eta}{\eta^2+\pi^2} - \int_0^\infty \frac{d\rho\exp(-\rho\omega)}{(\rho+\eta)^2+\pi^2}\right], \tag{26}$$

and we have introduced $\eta = \ln(\mu^2/\Lambda^2_{QCD})$ assuming $\mu > \Lambda_{QCD}$.

The first term in the square brackets in Eq. (26) corresponds to the imaginary part of Eq. (24) and the second one comes from the imaginary part of $1/(s - \mu^2 + \imath\epsilon)$.

The expression corresponding to graph (b) in Fig. 4 is

$$\frac{1}{8\pi^2}\left[\frac{1}{\omega} + \lambda\right](F_0^\pm)^2. \tag{27}$$

Here, the softest partons (i.e. partons with minimal $k_\perp$) here are given by the intermediate quark pair. The remaining graphs, (c) - (f) in rhs of Fig. 4, correspond to the case when the softest parton is a gluon and therefore can be factorized out, i.e. its propagator can be attached to the external lines in all possible ways.

The amplitude M_0 in the lhs of Fig. 4 is colourless, i.e. it belongs to the singlet representation of the group $SU_c(3)$. As one of the virtual gluons is removed from the blobs in graphs (c) - (f), these blobs are nolonger colourless. They correspond to the colour octet scattering amplitude M_8, where $k_\perp$ acts as a new IR cut-off. As M_8 does not depend on the longitudinal components of k, one can integrate over them, easily arriving at

$$\Im M^\pm_{(c-f)} = C_F\int_{\mu^2}^s \frac{d(-k^2)}{(-k^2)}\alpha_s(k^2)\Re_s M_8^\mp(\frac{s}{-k_\perp^2}). \tag{28}$$

Equation (28) reads that there is total compensation between the cuts of M_8, so that only cuts that do not involve M_8 (i.e. two-quark ones) contribute to $\Im M^\pm_{(c-f)}$.

As we are going to obtain $M_0^{(-)}$ to all orders in α_s with SL accuracy, we must first know $M_8^{(+)}$ with the same accuracy. However, for an evaluation of the asymptotic behaviour

of $M_0^{(-)}$, this knowledge is not necessary. Indeed, it was shown in ref. [17] that in DLA the blobs in Fig. 4c - f can be approximated, with a few percent accuracy, by their Born contribution. The reason is that the octet amplitude $M_8^{(+)}$ decreases with energy so quickly that higher-loop contributions can be neglected. Motivated by this result and noticing from the results of ref. [8] that, apart from running α_s effects, SL contributions do not change DL results drastically, we use this approximation in the present work, replacing the blobs in graphs (c) - (f) of the equation in Fig. 4 by their Born value, although with the running α_s. Substituting the Born approximation M_8^{Born} for the colour octet amplitude M_8,

$$\begin{aligned}\Re M_8^{\mp} &\approx \Re M_{8\,Born}^{\mp} = -2\pi\Re\left[\alpha_s(s)\frac{s}{s-\mu^2+\imath\epsilon} \mp \alpha_s(-s)\frac{-s}{-s-\mu^2+\imath\epsilon}\right] \\ &\approx -2\pi\left[\Re\alpha_s(s) \mp \Re\alpha_s(-s)\right], \end{aligned} \tag{29}$$

we then obtain

$$\Im M_{(c-f)}^{(\pm)} = -\frac{2\pi C_F}{2N}\left[\Re\alpha_s(s) - \Re\alpha_s(-s)\right]\int_{\mu^2}^{s}\frac{d(-k^2)}{(-k^2)}\alpha_s(k^2). \tag{30}$$

Finally, applying the Mellin transform Eq. (17) to Eq. (30), and using Eq. (24) for α_s, we obtain, for contribution of graphs (c) - (f) in Fig. 4:

$$D^{(\pm)}(\omega) = \frac{2C_F}{\omega b^2 N}\int_0^\infty d\rho e^{-\omega\rho}\ln\left(\frac{\rho+\eta}{\eta}\right)\left[\frac{\rho+\eta}{(\rho+\eta)^2+\pi^2} \mp \frac{1}{\rho+\eta}\right]. \tag{31}$$

In DLA, when α_s is fixed, instead of Eq. (31) one gets

$$D_{DL}^{(+)}(\omega) = 0 \quad , \qquad D_{DL}^{(-)}(\omega) = -\frac{4\alpha_s^2 C_F}{\omega^3 N} \quad . \tag{32}$$

The positive-signature contribution $D^{(+)}$ in the DLA is zero, so that M_8 does not contribute to $M_0^{(+)}$ at all. In the Feynman gauge this means that the positive-signature contribution of non-ladder graphs in the DLA is zero and only ladder graphs must be considered. This remarkable observation was first made in ref. [12] for QED processes, and later in [13] for quark scattering. Equation (31) shows that running α_s effects violate the total compensation of non-ladder graph contributions. In our previous work [8] we had neglected this non-compensation. We discuss it in more detail in Section 4.

Now we are able to write the full equation for $F_0^{(\pm)}$ shown in Fig. 4, which generalizes the equation for $F_0 = F_0^{(+)}$ obtained in our earlier work [8]:

$$F_0^{(\pm)}(\omega) = \frac{A(\omega)}{\omega} + \frac{1}{8\pi^2}\left[\frac{1}{\omega} + \lambda\right]\left(F_0^{(\pm)}(\omega)\right)^2 + D^{(\pm)}(\omega), \tag{33}$$

where $D^{(+)}$ and $D^{(-)}$ are given by Eq. (31); $\lambda = 1/2$ corresponds to SL contributions not related to running coupling effects.

Equation (33) has the following solution

$$F_0^{(\pm)} = 4\pi^2\,\frac{\omega - \sqrt{\omega^2 - (1+\lambda\omega)(A(\omega) + \omega D^{(\pm)}(\omega))/2\pi^2}}{1+\lambda\omega}\quad . \tag{34}$$

Combining this result with Eqs. (9), (18), (22) we finally obtain the following expressions for the structure functions f_1^{NS} and g_1^{NS}:

$$\begin{aligned} f_1^{NS} &= \int_{-\imath\infty}^{\imath\infty}\frac{d\omega}{2\pi\imath}C\left(\frac{1}{x}\right)^{\omega}\omega\exp\left(\left[(1+\lambda\omega)F_0^{(+)}/8\pi^2\right]y\right) \\ g_1^{NS} &= \int_{-\imath\infty}^{\imath\infty}\frac{d\omega}{2\pi\imath}C\left(\frac{1}{x}\right)^{\omega}\omega\exp\left(\left[(1+\lambda\omega)F_0^{(-)}/8\pi^2\right]y\right) \end{aligned} \tag{35}$$

with C arbitrary.

III. ASYMPTOTICS OF THE NON-SINGLET STRUCTURE FUNCTIONS

The small-x asymptotic behaviour of g_1^{NS} and f_1^{NS} can be obtained by evaluating the expressions found at the end of last section with the saddle-point method. However, it is much easier to get it directly, by noticing that at small x $g_1^{NS} \sim x^{-\omega_0^{(-)}}$ and $f_1^{(NS)} \sim x^{-\omega_0^{(+)}}$, where $\omega_0^{(\pm)}$ is the rightmost singularity of $F^{(\pm)}$. Equation (34) reads that this singularity is a square root branch point given by a solution to[2]

$$\begin{aligned} &\omega^2 - (1+\lambda\omega)\left\{\left(\frac{2C_F}{\pi b}\right)\left[\frac{\eta}{\eta^2+\pi^2} - \int_0^\infty \frac{d\rho e^{-\omega\rho}}{(\rho+\eta)^2+\pi^2}\right] + \right. \\ &\left.\left(\frac{2C_F}{\pi b}\right)^2\frac{1}{4NC_F}\int_0^\infty d\rho e^{-\omega\rho}\ln\left(\frac{\rho+\eta}{\eta}\right)\left[\frac{\rho+\eta}{(\rho+\eta)^2+\pi^2} \mp \frac{1}{\rho+\eta}\right]\right\} = 0\quad . \end{aligned} \tag{36}$$

---

[2]There is a misprint in the coefficient before the square brackets of Eq. (52) in ref. [8]. The true coefficient is $(2C_F/\pi b)$. However the numerical results of ref. [8] are correct.

We recall that $\rho = \ln(s/\mu^2)$ and $\eta = \ln(\mu^2/\Lambda^2_{QCD})$. This equation can be solved numerically. Before doing so, let us notice that if we keep α_s fixed in Eq. (36) and, for self-consistency, put $\lambda = 0$, it transforms into the well-known algebraic equation in the DLA:

$$\omega^2 - \frac{2\alpha_s C_F}{\pi} - \left(\frac{2\alpha_s C_F}{\pi}\right)^2 \frac{1}{4NC_F}\frac{1}{\omega^2}[1-(\pm 1)] = 0, \tag{37}$$

with the obvious solutions

$$\widetilde{\omega}^{DL}_{(-)} = \widetilde{\omega}^{DL}_{(+)}\sqrt{\frac{1}{2}\left[1+\left(1+\frac{4}{(N^2-1)}\right)^{1/2}\right]} \approx 1.055\ \widetilde{\omega}^{DL}_{(+)}, \tag{38}$$

where the positive-signature leading singularity reads:

$$\widetilde{\omega}^{DL}_{(+)} = \sqrt{2\alpha_s^{DL} C_F/\pi}\ \ . \tag{39}$$

Now let us come back to Eq. (35). Substituting the value of $F_0^{(\pm)}$ of Eq. (34) at the point $\omega = \omega_0^{(\pm)}$, where the square root turns to zero, we arrive at the power-like asymptotics:

$$\begin{aligned} f_1^{NS} &\sim \left(\frac{1}{x}\right)^{\omega_0^{(+)}} \left(\frac{Q^2}{\mu^2}\right)^{\omega_0^{(+)}/2}, \\ g_1^{NS} &\sim \left(\frac{1}{x}\right)^{\omega_0^{(-)}} \left(\frac{Q^2}{\mu^2}\right)^{\omega_0^{(-)}/2}\ \ . \end{aligned} \tag{40}$$

Obviously, the solutions $\omega_0^{(+)}$ and $\omega_0^{(-)}$ to Eq. (36) (also called the intercepts of f_1^{NS} and g_1^{NS}, respectively) depend on the choice of the parameters n_f, μ, Λ_{QCD}. We recall that we keep $\mu > \Lambda_{QCD}$. Also, μ must be greater than the mass of the heaviest involved quark, which fixes n_f. In numerical estimates below, we have used $\Lambda_{QCD} = 0.1$ GeV and $n_f = 3$. Equation (36) has been solved numerically for different values of μ. The dependence of the intercepts $\omega_0^{(\pm)}$ on μ (in terms of η) is plotted in Fig. 5. The plot shows that $\omega_0^{(-)}$ is greater than $\omega_0^{(+)}$ for all μ. Both $\omega_0^{(+)}$ and $\omega_0^{(-)}$ first grow with increasing μ, getting maximal at $\mu \approx 1$ GeV , where

$$\omega_0^{(+)} \equiv \Omega^{(+)} = 0.37 \tag{41}$$

and

$$\omega_0^{(-)} \equiv \Omega^{(-)} = 0.4, \tag{42}$$

and smoothly fall off after that. Equation (36) also tells us that contrary to the double-logarithmic approximation of Eq. (38), there is no total compensation between the DL contributions of the non-ladder graphs to $\omega_0^{(+)}$ (see expression in the second squared brackets) when α_s is running. That fact was neglected in [8]. Once taken into account, it leads to a steep increase of both $\omega_0^{(+)}$ and $\omega_0^{(-)}$ at small η. However, we regard this increase as an artefact of our approach: using expression (24) for α is becoming unreliable at such small η. Another reason for not considering the small-η region is that when $\eta \leq 2.86$ the values of $\omega_0^{(+)}$ become complex, which leads to negative f_1^{NS}. Thus, we find that our approach is valid for $\eta \geq 2.8$. Recalling that $\eta = \ln[(\mu/\Lambda_{QCD})^2]$, with μ acting as an input for our evolution equations, we see that, for self-consistency, we must keep $\mu \geq \mu_{min} = 17.5\Lambda_{QCD} = 1.75$ GeV as $\Lambda_{QCD} = 0.1$ GeV. A further look at Fig. 5 shows that $\omega_0^{(+)}$ and $\omega_0^{(-)}$ are maximal at $\eta \approx 5$. Then they smoothly ($\sim 1/\eta$) fall with growing η. The reason for this fall-off is quite clear: at large η, the running α_s is approximated by $1/(b\eta)$. The η-dependence of $\omega_0^{(\pm)}$, plotted in Fig. 5, has such a complicated form because of the competition between the relative weights of the π^2- and η-contributions in the denominators of Eq. (36). In the absence of the π^2-terms $\omega_0^{(\pm)}$ will depend on η in a smoother way, as shown by the curves (3) and (4) in Fig. 5. We will further discuss this plot in the next section.

IV. COMPARING WITH THE LEADING LOGARITHMIC APPROXIMATION

The power-like (Regge-like) small-x behaviour of f_1^{NS} and g_1^{NS}, Eq. (40), with DL intercepts $\omega_0^{(\pm)} = \widetilde{\omega}_{(\pm)}^{DL}$ given by Eqs. (38) and (39), was obtained in refs. [5] and [6]. These expressions explicitly include the dependence of α_s upon an unknown scale, because the DL approximation treats α_s as fixed. On the other hand, the LLA approach postulates that asymptotically, at very high energies, LLA results should dominate over all sub-leading contributions. Having accounted for the SL contributions, we are now able to check the validity of the LLA predictions for the NS structure functions. First, let us notice that accounting

for running α_s does not lead to intercepts $\omega_0^{(\pm)}$ explicitly dependent on α_s, although they depend on Λ_{QCD}. Then, thanks to our choice of the infrared regulation, Eq. (13), $\omega_0^{(\pm)}$ depend on μ. But in spite of such a difference between $\omega_0^{(\pm)}$ and the DL intercepts $\widetilde{\omega}_{(\pm)}^{DL}$, one can see from Eq. (38) and Fig. 5 that the DL ratio $\left[\widetilde{\omega}_{(-)}^{DL} - \widetilde{\omega}_{(+)}^{DL}\right] / \widetilde{\omega}_{(+)}^{DL} = 0.055$ basically holds for $\omega_0^{(\pm)}$ also, changing slightly from 0.09 at $\eta = 3$ to 0.06 at $\eta = 8$. Therefore, the DL result for the ratio in Eq. (38) is a good approximation. The π^2-terms that we have accounted for in Eq. (36)are quite important because of their large value. In principle, they are formally beyond the SL accuracy we have kept through the paper. Indeed, contributions $\sim \pi^2$ may appear also from integrations over phase space. Such contributions in higher orders of the perturbative series are beyond the control of any kind of logarithmic approximation. On the other hand the π^2 we have accounted for appear as the result of respecting the analytical properties of the scattering amplitudes. So, we cannot simply neglect them. Moreover, it has been shown recently in ref. [18] that a value $\Omega^{(-)} = 0.4$ is in good agreement with the experimental data for the structure function F_3 . When the π^2 in Eq. (36) are dropped, $\Omega^{(-)} = 0.4$ corresponds to $\mu \approx 5.5$ GeV (see curves 3 and 4 in Fig. 5). At this value of μ the SL contributions not related to the running α_s are small, i.e. one can neglect them, putting $\lambda = 0$ in Eq. (36). Therefore we conclude that $\mu_0 \equiv 5.5$ GeV is a good estimate of the value of the mass scale for LLA evolution equations. In other words, μ_0^2 acts as a momentum scale for the evolution equations obtained in LLA. Therefore these equations are not expected to reproduce the correct Q^2-dependence until at least

$$Q^2 > \mu_0^2 \approx 30 \text{ GeV}^2 \quad . \tag{43}$$

As μ_0^2 is pretty close to the typical values of Q^2 at HERA, we can see that using the LLA evolution equations is not very reliable for such Q^2.

Let us discuss the x-dependence. In refs. [19–21], it is assumed that α_s depends on Q^2 in the expression for the intercepts. On the other hand the results of ref. [8] show that there is no such dependence. Now we have seen that in LLA α_s should depend rather on μ_0^2 than on Q^2, and as the Q^2 range covered at HERA is not far from μ_0^2 the estimate $\alpha_s = \alpha_s(Q^2)$

might still be in reasonable agreement with the data.

V. COMPARISON WITH DGLAP

Now let us compare our results with the DGLAP results for the non-singlet structure functions. First, let us check that the corresponding DGLAP evolution equations can be obtained from Eq. (21). Writing Eq. (21) as

$$\frac{\partial}{\partial y}F^{(\pm)}(\omega,y)=\left[-\omega+\frac{1}{8\pi^2}(1+\lambda\omega)\right]F_0^{(\pm)}(\omega)F^{(\pm)}(\omega,y) \tag{44}$$

and noting that the term $-\omega$ in the square brackets is absorbed by changing the Mellin factor $(s/\mu^2)^\omega$ to $x^{-\omega}$ (see Eq. (35)), then

$$\widetilde{\gamma}^{(\pm)}=\frac{1}{8\pi^2}(1+\lambda\omega)F_0^{(\pm)}(\omega) \tag{45}$$

are the new small-x non-singlet anomalous dimensions. However, when $x\sim 1$ the main contribution of the Mellin factor $\exp[\omega\ln(1/x)]$ comes from the region of rather large values of ω, where $\omega\ln(1/x)\leq 1$. That makes it possible to expand the exponent $F_0^{(\pm)}$ in Eq. (35) into a series in $1/\omega$. Doing so, we obtain

$$\widetilde{\gamma}^{(\pm)}\approx(1+\lambda\omega)\frac{F_0^{(\pm)}}{8\pi^2}=\frac{A}{8\pi^2}\left[\frac{1}{\omega}+\lambda\right]+\left(\frac{A}{8\pi^2}\right)^2\frac{1}{\omega}\left[\frac{1}{\omega}+\lambda\right]^2+D^{(\pm)}+O(A^3)\quad . \tag{46}$$

Retaining only the first term in the rhs of Eq. (46), one arrives at the expression

$$\widetilde{\gamma}^{(\pm)}_{(1)}=\frac{A}{8\pi^2}\left[\frac{1}{\omega}+\lambda\right] \tag{47}$$

for the leading order anomalous dimension, which is similar to the expression for the leading order DGLAP non-singlet anomalous dimension

$$\gamma_{(1)}=\frac{\alpha_s(Q^2)C_F}{2\pi}\left[\frac{1}{\omega}+\lambda\right]\quad . \tag{48}$$

Let us first compare the two results by assuming that α_s is fixed. Equations (47) and (48) coincide completely because in this case $A=4\pi\alpha_s C_F$. Let us then compare the next

two terms in Eq. (46) with the second order DGLAP anomalous dimension $\gamma_{(2)}^{(\pm)}$, again for fixed α_s. Retaining the leading terms, proportional to $1/\omega^3$, we can see that

$$\tilde{\gamma}_{(2)}^{(\pm)} = \left(\frac{A}{8\pi^2}\right)^2 \frac{1}{\omega}\left[\frac{1}{\omega} + \lambda\right]^2 + D^{(\pm)} \tag{49}$$

transform into (see Eq. (32))

$$\gamma_{(2)}^{(+)} = \left(\frac{\alpha_s}{\pi}\right)^2 \frac{C_F^2}{2}\frac{1}{\omega^3} \tag{50}$$

and

$$\gamma_{(2)}^{(-)} = \left(\frac{\alpha_s}{\pi}\right)^2 \left[\frac{C_F^2}{2} + \frac{C_F}{N}\right]\frac{1}{\omega^3}, \tag{51}$$

which coincide with the leading terms of Eq. (B18) of ref. [10], also used in ref. [9] for the second order non-singlet anomalous dimensions. Unfortunately, we do not obtain exact coincidence between non-leading terms, which are proportional to $1/\omega^3$, but this can be explained by a different choice of the factorization and regularization procedures. Therefore, the non-singlet anomalous dimensions given by Eq. (45) correspond to a resummation of $\gamma_{(1)}$ to all orders in the QCD coupling and to accounting for the signature-dependent DL contributions to order α_s^2. Such a resummation leads to the power-like small-x behaviour, which cannot be achieved by incorporating any finite number of NLO contributions into expressions for DGLAP anomalous dimensions.

Another difference between IREE and DGLAP is the different treatment of the QCD coupling. Although both approaches use the same formula (Eq. (24)) for α_s, the DGLAP uses $\alpha_s = \alpha_s(k_{i\perp}^2)$ in i-th ladder rung, $k_{i\perp}$ being the ladder quark transverse momentum whereas IREE suggests that in the i-th rung α should depend on the gluon virtuality [3] $(k_i - k_{i-1})^2$. Let us explain this difference. When $x \neq 1$, the Born contribution to f^{NS} is zero and f^{NS} obeys the Beth - -Salpeter equation

---

[3]We use here the standard numeration for the momenta of the virtual ladder quarks k_i, so that $i = 0$ corresponds to $k_0 = p$ and, increasing the number of runs, it leads to the top of the ladder.

$$f^{NS} = \int d^4k \Phi((q+k)^2) \frac{1}{k^2} \Im \frac{\alpha_s((p-k)^2)}{[(p-k)^2]} \quad . \tag{52}$$

We have suppressed all unimportant factors in Eq. (52) and have used the notation k instead of k_1 for the ladder quark momentum in the lowest rung. We have noted as Φ for off-shell f^{NS}. Usually it is convenient to integrate over k in (52), using the Sudakov parametrization:

$$k_\nu = \alpha(q + xP)_\nu + \beta p_\nu + k_\perp, \tag{53}$$

so that

$$2(pk) = 2(pq)\alpha, \quad 2(qk) = 2(pq)(\beta - x\alpha), \quad k^2 = 2(pq)\alpha\beta - k_\perp^2 \quad . \tag{54}$$

But here it is more convenient to use the variable

$$m^2 \equiv (p-k)^2 \tag{55}$$

instead of the Sudakov variable α, writing Eq. (52) as

$$f^{NS} = \int d^2k_\perp d\beta dm^2 \Phi\Big(\Big[s(\beta - x)(1-\beta) - m^2(\beta - x) - k_\perp^2(1-x)\Big](1-\beta)^{-1}\Big) \cdot \Im \frac{\alpha_s(m^2)}{[\beta m^2 + k_\perp^2][m^2]} \quad . \tag{56}$$

The argument of Φ in Eqs. (52) and (56) should be positive, i.e.

$$\Big[s(\beta - x)(1-\beta) - m^2(\beta - x) - k_\perp^2(1-x)\Big] \geq 0 \; . \tag{57}$$

When $x \sim 1$, one can neglect the last term in Eq. (57). It leads to $(\beta - x)(s(1-\beta) - m^2) \geq 0$, which allows m^2 to be neglected. Therefore, instead of Eq. (56), we obtain

$$f^{NS} = \int d^2k_\perp d\beta dm^2 \Phi\left([s(\beta - x)(1-\beta)](1-\beta)^{-1}\right) \Im \frac{\alpha_s(m^2)}{[\beta m^2 + k_\perp^2][m^2]} \quad . \tag{58}$$

After that, one can apply the Cauchy theorem relating an analytic function to its imaginary part. This permits to perform an integration over m^2 by taking residues. As m^2 is positive, the only residue is $m^2 = -k^2/\beta$. Thus, we obtain

$$f^{NS} = \int d^2k_\perp d\beta \Phi\left([s(\beta - x)(1-\beta)](1-\beta)^{-1}\right) \frac{\alpha_s(-k_\perp^2/\beta)}{k_\perp^2} \quad . \tag{59}$$

As $\beta \geq x$ and $x \sim 1$, one can drop β in the argument of α_s and arrive at

$$f^{NS} = \int d^2k_\perp d\beta \Phi \left([s(\beta - x)(1-\beta)] (1-\beta)^{-1} \right) \frac{\alpha_s(-k_\perp^2)}{k_\perp^2} \quad , \tag{60}$$

which corresponds to the DGLAP. Usually the negative sign of the argument of α_s is dropped together with the negative sign of the argument in Eq. (24). As the argument of α_s in Eq. (59) is negative, the expression for α_s in the DGLAP approximation of Eq. (60) does not contain π^2-terms at all, while the argument of α_s in Eq. (52) is positive and therefore there are π^2-terms in Eq. (52).

Obviously, the transition from Eq. (52) to Eq. (59) holds only when $x \sim 1$, which is the DGLAP kinematics, and fails for small x. In particular, neglecting $k_\perp^2$ in Eq. (57) has an important consequence for the DGLAP evolution, where one picks up logarithmic contributions through integrations over $k_\perp$. At small x one should use the α_s-dependence given by Eq. (26) rather than that given by Eq. (60).

VI. CONCLUSIONS

In conclusion, we have obtained a generalization of the second-order DGLAP evolution equations for the non-singlet structure functions at small x. Besides resumming the LO DGLAP anomalous dimension to all orders in α_s and accounting for running α_s effects, we account for the difference between f_1^{NS} and g_1^{NS}, which is due to the difference in the second-order anomalous dimensions. We have shown that, with single-logarithmic contributions and running α_s taken into account, f_1^{NS} and g_1^{NS} have the scaling-like asymptotic behaviour

$$\sim x^{-\omega_0^{(\pm)}} \left(\frac{Q^2}{\mu^2} \right)^{(\omega_0^{(\pm)}/2)} , \tag{61}$$

as also obtained earlier in the DLA [5,6] at asymptotically small x. We have appropriately calculated the intercepts $\omega_0^{(\pm)}$. We have made detailed comparisons of our results with the predictions obtained in the leading-logarithmic approximation and with the DGLAP. Results obtained with the evolution equations usually depend on a mass scale μ_0^2 acting as a starting

point of the evolution with respect to Q^2, and we estimate the value for this mass scale for a LLA evolution equation as $\mu_0^2 \approx 30$ GeV^2. This implies that these equations can reproduce the correct Q^2-dependence for the non-singlet structure functions (and likely, for the singlet ones) only for approximately $Q^2 > 30$ GeV^2 . On the other hand, as far as the x-dependence is concerned, we have also shown that the estimate $\alpha_s = \alpha_s(Q^2)$ used in refs. [19–21] in LLA can be in a reasonable agreement with the x-behaviour of the structure functions for the HERA data.

VII. ACKNOWLEDGEMENTS

The work is supported in part by grant INTAS-97-30494, and by EU QCDNET contract FMRX-CT98-0194.

REFERENCES

[1] R.P.Feynman, Photon-hadron interactions (Benjamin, 1972); B.L.Ioffe, V.A.Khoze and L.N.Lipatov, Hard Processes (North Holland, 1984).

[2] G.Altarelli and G.Parisi, Nucl. Phys. B126 (1977) 297; V.N.Gribov and L.N.Lipatov, Sov. J. Nucl. Phys. 15 (1972) 438; L.N.Lipatov, Sov. J. Nucl. Phys. 20 (1972) 95; Yu.L.Dokshitzer, Sov. Phys. JETP 46 (1977) 641.

[3] G.Altarelli, R.D.Ball, S.Forte and G.Ridolfi, Nucl. Phys. B496 (1997) 337.

[4] V.S.Fadin, E.A.Kuraev and L.N.Lipatov, Sov. Phys. JETP 44 (1976) 443 and 45 (1977) 199; Y.Y.Balitskij and L.N.Lipatov, Sov. J. Nucl. Phys. 28 (1978) 822.

[5] B.I.Ermolaev, S.I.Manayenkov and M.G.Ryskin, Z. Phys. C69 (1996) 259.

[6] J.Bartels, B.I.Ermolaev and M.G.Ryskin, Z. Phys. C70 (1996) 273 and C72 (1996) 627.

[7] S.J.Brodsky, V.S.Fadin, V.T.Kim, L.N.Lipatov and G.B.Pivovarov, JETP Lett. 70 (1999) 155-160; hep-ph/9901229.

[8] B.I.Ermolaev, M.Greco and S.I.Troyan, Nucl. Phys. B571 (2000) 137; hep-ph/9906276.

[9] M.Gluck, E.Reya, M.Stratmann and W.Vogelsang, Phys.Rev. D53 (1996) 4775.

[10] E.G.Floratos, C.Kounnas and R. Lacaze, Nucl. Phys. B 192 (1981) 417.

[11] P.D.B.Collins, An introduction to Regge theory and high energy physics. Cambridge, 1977.

[12] V.G.Gorshkov, L.N.Lipatov and M.M.Nesterov, Yad. Fiz. 9 (1969) 1321.

[13] R.Kirschner and L.N.Lipatov, Nucl. Phys. B213 (1983) 122.

[14] L.N.Lipatov, Phys. Lett. B116 (1982) 411.

[15] B.I.Ermolaev and L.N.Lipatov, Int. J. Mod. Phys. A4 (1989) 3147.

[16] B.I.Ermolaev, V.S.Fadin and L.N.Lipatov, Sov. J .Phys. 45 (1987) 508.

[17] B.I.Ermolaev and S.I.Troyan, in Proceedings of 5th Intern. Workshop on DIS, New York 1998, p. 861.

[18] A.Kataev, G.Parente and A.V.Sidorov. Nucl. Phys. A666/667 (2000) 184; Nucl. Phys. B573 (2000) 405.

[19] B.Badalek and J.Kwiecinski, Phys. Lett. B418 (1998) 229.

[20] J.Kwiecinski and B.Ziaja, hep-ph/9902440.

[21] Y.Kiyo and J.Kodaira, hep-ph/9803448; hep-ph/9711260; Z. Phys. C74 (1997) 631.

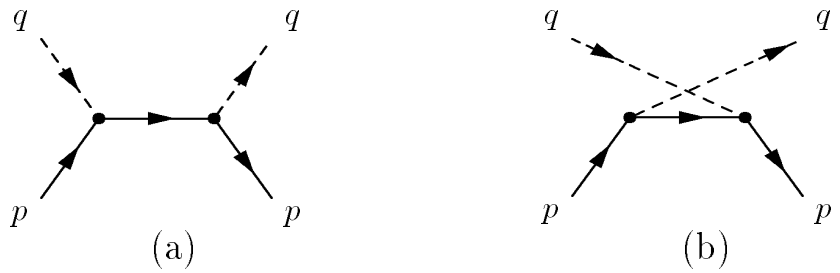

FIG. 1. The Born graphs for the DIS amplitude $M_{\mu\nu}$.

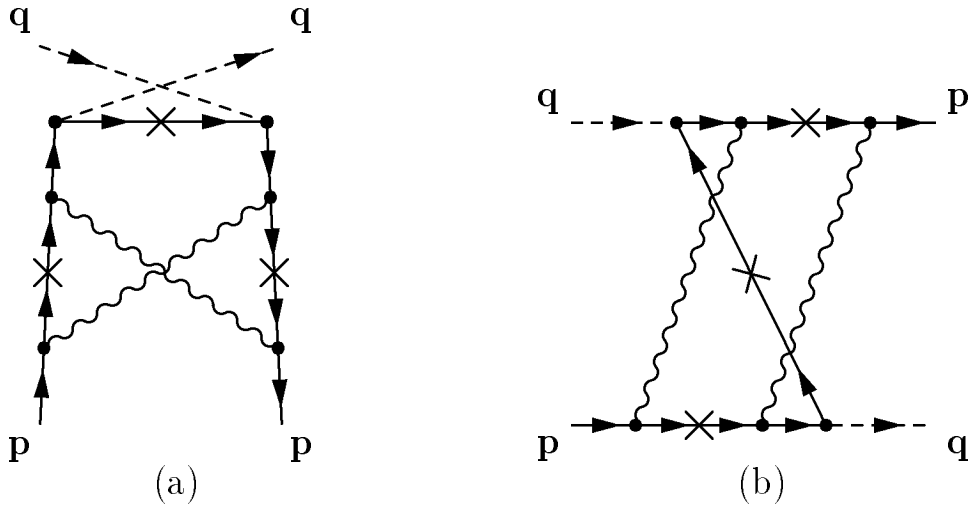

FIG. 2. Two-loop graph obtained from Fig. 1b, contributing to $\Im_s M^{(-)}_{\mu\nu}$ (a), and the corresponding physical process (b).

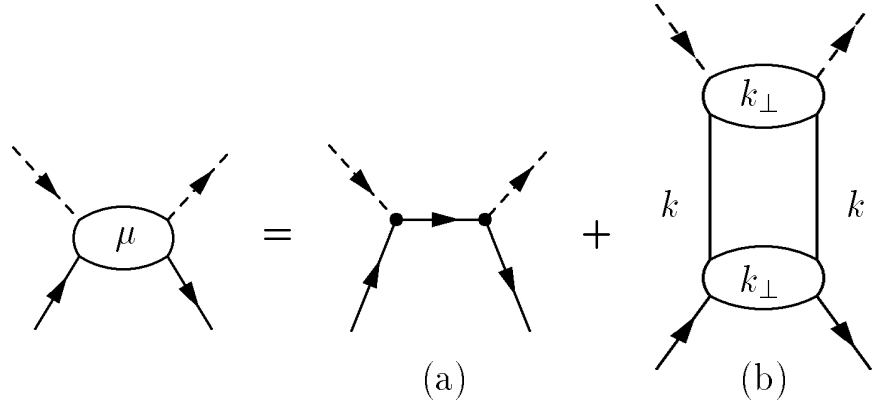

FIG. 3. The evolution equation for the DIS amplitude $M_{\mu\nu}$.

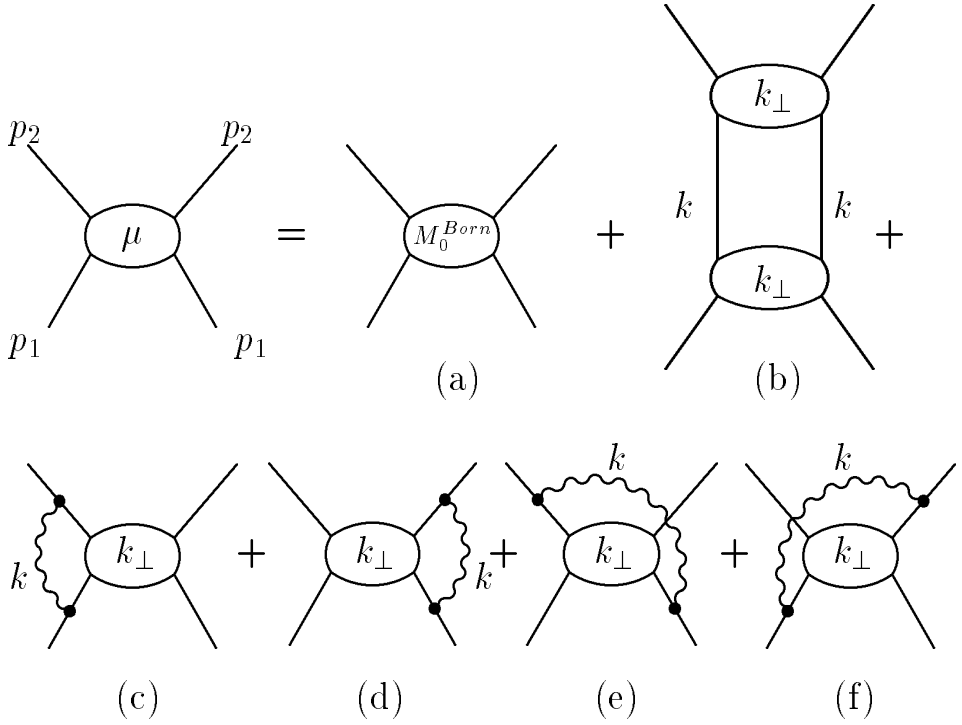

FIG. 4. The evolution equation for the quark scattering amplitude M_0.

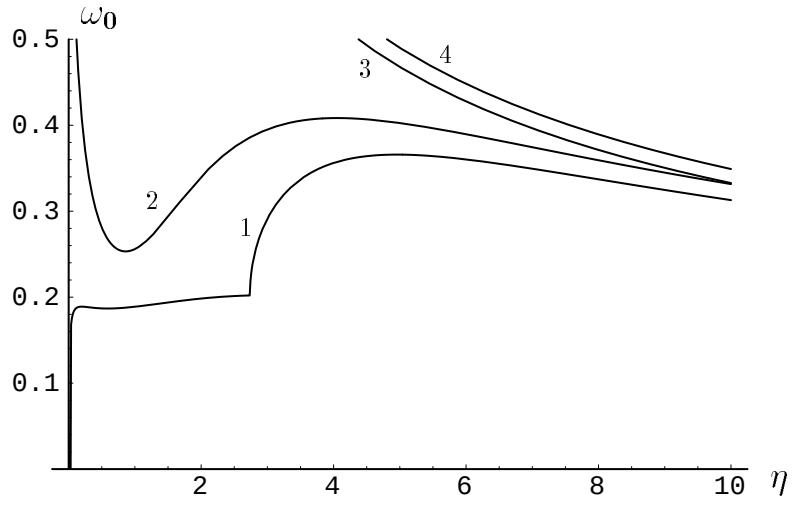

FIG. 5. Dependence of the intercept ω_0 on infrared cut-off $\eta = \ln(\mu^2/\Lambda_{QCD})$. 1: for f_1^{NS}, 2: for g_1^{NS}, 3 and 4: for f_1^{NS} and g_1^{NS}, respectively, without accounting for π^2-terms.